Contrib Mineral Petrol (2001) 141: 36–52
DOI 10.1007/s004100000223

A. Polat · R. Kerrich

Magnesian andesites, Nb-enriched basalt-andesites, and adakites from late-Archean 2.7 Ga Wawa greenstone belts, Superior Province, Canada: implications for late Archean subduction zone petrogenetic processes

Received: 6 December 1999 / Accepted: 31 October 2000 / Published online: 9 February 2001

Abstract Magnesian andesites (MA) occur with 'normal' tholeiitic to calc-alkaline basalt-andesite suites in four greenstone belts of the 2.7 Ga Wawa subprovince, Canada. Collectively, the magnesian andesites span ranges of SiO_2 = 56–64 wt%, Mg-number = 0.64–0.50, with Cr and Ni contents of 531–106 and 230–21 ppm, respectively. Relative to 'normal' andesites, the magnesian andesites form distinct trends on variation diagrams, with relatively high Th and LREE contents, uniform Yb over a range of MgO, more fractionated HREE, and lower Nb/Th_{pm} and Nb/La_{pm} ratios. Niobium-enriched basalts and andesites (NEBA; Nb = 7–16 ppm), and an Al-enriched rhyolite (adakite) suite are associated in space and time with the magnesian andesites. Nb-enriched basalts and andesites are characterized by high TiO_2, P_2O_5, Th, and Zr contents, variably high Zr/Hf (36–44) ratios, and more fractionated HREE (Gd/Yb_{cn} = 1.3–4.1) compared to the 'normal' tholeiitic to calc-alkaline basalt-andesite suites. The adakite suite has the high Al (Al_2O_3 = 16–18 wt%), high La/Yb_{cn} (21–43), and low Yb (0.4–1.2 ppm) of Archean tonalite-trondhjemite-granodiorite (TTG) suites and Cenozoic adakites, indicative of liquids derived mainly from slab melting. The basalt-andesite suites are not characterized by normal tholeiitic or calc-alkaline fractionation trends of major or trace elements. Rather, compositional trends can be accounted for by some combination of fractional crystallization and variable degrees of metasomatism of the source of basalt and/or andesites by adakitic liquids. The occurrence of magnesian andesites, Nb-enriched basalts/andesites, and adakites has been described from certain Phanerozoic arcs featuring shallow subduction of young and/or hot oceanic lithosphere. Adakites likely represent slab melts, magnesian andesites the product of hybridization of adakite liquids with mantle peridotite, and Nb-enriched basalts/andesites melts of the residue from hybridization. Geological similarities between the late-Archean Wawa greenstone belts and certain Cenozoic transpressional orogens with the MA-NEBA-adakite association suggest that subduction of young, hot oceanic lithosphere may have played an important role in the production of this arc-related association in the late Archean.

A. Polat (✉) · R. Kerrich
Department of Geological Sciences,
University of Saskatchewan,
Saskatchewan S7 N 5E2,
SK, Canada
E-mail: polat@mpch-mainz.mpg.de

A. Polat
Present address: Max-Planck-Institut für Chemie,
Postfach 3060, 55020 Mainz,
Germany

Editorial responsibility: A. Hofmann

Introduction

Volcanic successions in late Archean greenstone belts of the Superior Province, and Archean greenstone belts in general, are dominated by two associations. Tholeiitic basalts with near-flat REE patterns and komatiites form one association (Sun and Nesbitt 1978; Arndt and Nesbitt 1982; Xie et al. 1993; Polat et al. 1998; Kerrich et al. 1999a), whereas bimodal basalts and dacites to rhyolites constitute the second (Condie 1981; Thurston et al. 1985; Laflèche et al. 1992). The former are interpreted largely as intra-oceanic plateau sequences, whereas the latter are as intra-oceanic arcs (Polat et al. 1998).

Andesites are rare in Archean greenstone volcanic successions, and there are still fewer known magnesian andesites (Taylor and McLennan 1985; Condie 1986; Thurston 1990). This paper reports geochemical data for recently recognized but rare magnesian andesites (MA) in four calc-alkaline basalt-andesite arc volcanic successions of the 2.7 Ga Wawa subprovince of the Superior Province. Greenstone belts sampled for this study include the Schreiber-Hemlo, White River-Dayohessarah, Winston-Big Duck Lake, and Manitouwadge belts. Associated with the magnesian andesites are Nb-enriched basalts and andesites (NEBA; Nb = 7–16 ppm),

and adakites (aluminous dacites to rhyolites) with compositions akin to Archean high-Al, tonalite-trondhjemite-granodiorite (TTG) suites, and Cenozoic adakites, both of which are considered to be slab-derived melts (cf. Drummond et al. 1996). Compositional boundaries between these suites are transitional for many elements.

Structural studies indicate that Wawa greenstone belts underwent a complex history of faulting, folding, and fabric development, resulting in destruction of original stratigraphic relationships between different lithological units (Polat et al. 1998; Polat and Kerrich 1999). Consequently, the presently exposed abundance of each unit or magmatic suite may not reflect the original relative abundance.

Geochemical characteristics of volcanic rocks in Archean greenstone belts have been shown to be useful in providing information concerning the petrogenesis, tectonic setting, and geodynamic evolution of these belts (e.g., Condie 1981; Laflèche et al. 1992; Polat et al. 1998, 1999, and references therein). Accordingly, the purpose of this study is to document the composition of the newly recognized, volcanic suites present, and compare these to counterparts in Cenozoic arcs where the spatial and temporal relationships of the arc basalt-andesite, magnesian andesite, adakite, Nb-enriched basalt-andesite association is well constrained in a plate-tectonic context. Structural and geochemical analyses of areally extensive, plume-related tholeiitic basalts and komatiites as well as arc-related magmas and associated siliciclastic trench turbidites in Wawa subprovince greenstone belts have been the subject of separate studies (Polat et al. 1998, 1999; Polat and Kerrich 1999).

Geological setting

The Superior Province, the largest Archean craton globally, is composed of plutonic, volcanic-plutonic, high-grade gneiss and metasediment-dominated subprovinces (Fig. 1; Card and Ciesielski 1986; Card 1990; Thurston et al. 1991; Percival et al. 1994). The total range of ages of these various subprovinces is from 3.1–2.67 Ga. These subprovinces are considered to have been amalgamated by accretionary tectonics over a period of 2.74–2.65 Ga (Card and Ciesielski 1986; Card 1990; Percival et al. 1994). Extensive geochronological studies on their prekinematic, synkinematic, and postkinematic igneous rocks reveal that the assembly of these subprovinces was diachronous from north to south (Thurston 1990; Percival et al. 1994; Stott 1997).

Greenstone belts in the Archean Superior Province are 1–100-km-scale areas of supracrustal rocks within composite granitoid-greenstone terranes with tectonic or intrusive boundaries. A greenstone belt may consist of one or more lithotectonic assemblages, each characterized by stratified volcanic and/or sedimentary rock units built during a discrete interval of time in a common depositional or volcanic setting (Thurston et al. 1991).

The Schreiber-Hemlo, White River-Dayohessarah, Winston-Big Duck Lake, and Manitouwadge greenstone belts are located in the northeastern section of the volcanic-plutonic Wawa subprovince of the Superior Province, which extends from the Vermilion district of Minnesota in the west to the Kapuskasing structural zone in the east (Fig. 1; Williams et al. 1991). According to Williams et al. (1991), these greenstone belts can be divided into various lithotectonic assemblages. The Schreiber-Hemlo greenstone belt is divided into three lithotectonic assemblages, i.e., the Schreiber (SC), Hemlo-Black River (HEBR), and Heron Bay (HB) assemblages. The Schreiber and Hemlo-Black River assemblages are separated by the Proterozoic Coldwell alkali complex (Fig. 1). The Hemlo-Black River and Heron Bay assemblages are located to the north and south of the right-lateral Lake Superior-Hemlo fault zone (LSHFZ), respectively (Fig. 1). Similarly, the Winston-Big Duck Lake belt is divided into two lithotectonic assemblages, these being the Winston Lake and Big Duck Lake assemblages. The White River-Dayohessarah and Manitouwadge greenstone belts have not been divided into distinct lithotectonic assemblages. All these assemblages are composed of similar volcanic and siliciclastic sedimentary rocks, and are multiply intruded by synkinematic, high-Al, high-La/Yb_{cn} TTG plutons, and late-kinematic lamprophyre dikes (Williams et al. 1991; Zaleski and Peterson 1995; Polat et al. 1998; Polat and Kerrich 1999).

Stratigraphic relationships between different lithological units are commonly obscure and often marked by shear zones. Volcanic rocks consist mainly of tholeiitic ocean plateau basalts, including both pillow basalts and massive flows, komatiites and komatiitic basalts with well preserved spinifex texture, and oceanic island arc tholeiitic to calc-alkaline basalts, andesites, dacites, and rhyolites (Polat et al. 1998). There are minor cherts, iron formations, and gabbros within these volcanic sequences. Although the original stratigraphic relationships between different volcanic rocks have been disrupted and complicated by subsequent deformation (Polat and Kerrich 1999), in a few areas (e.g., Hemlo, Heron Bay) it appears that the tholeiitic basalt-komatiite oceanic plateau association occurs mainly at the base of volcanic sequences, whereas tholeiitic to calc-alkaline bimodal volcanic arc sequences are more abundant at the upper tectonostratigraphic levels.

Sedimentary rocks consist of interbedded turbiditic greywacke sandstones, siltstones, and shales (Williams et al. 1991; Muir 1997; Polat et al. 1998). Conglomerates are minor, occurring primarily in turbidite channels. Primary sedimentary structures (e.g., parallel bedding, cross-bedding, and grading) are intensely deformed and transposed to a large extent throughout the belt.

The greenstone belts are typically metamorphosed at greenschist to amphibolite facies. Amphibolite facies metamorphism occurs primarily proximal to TTG batholiths. Regional metamorphic studies suggest an apparent northward increase in metamorphic grade in

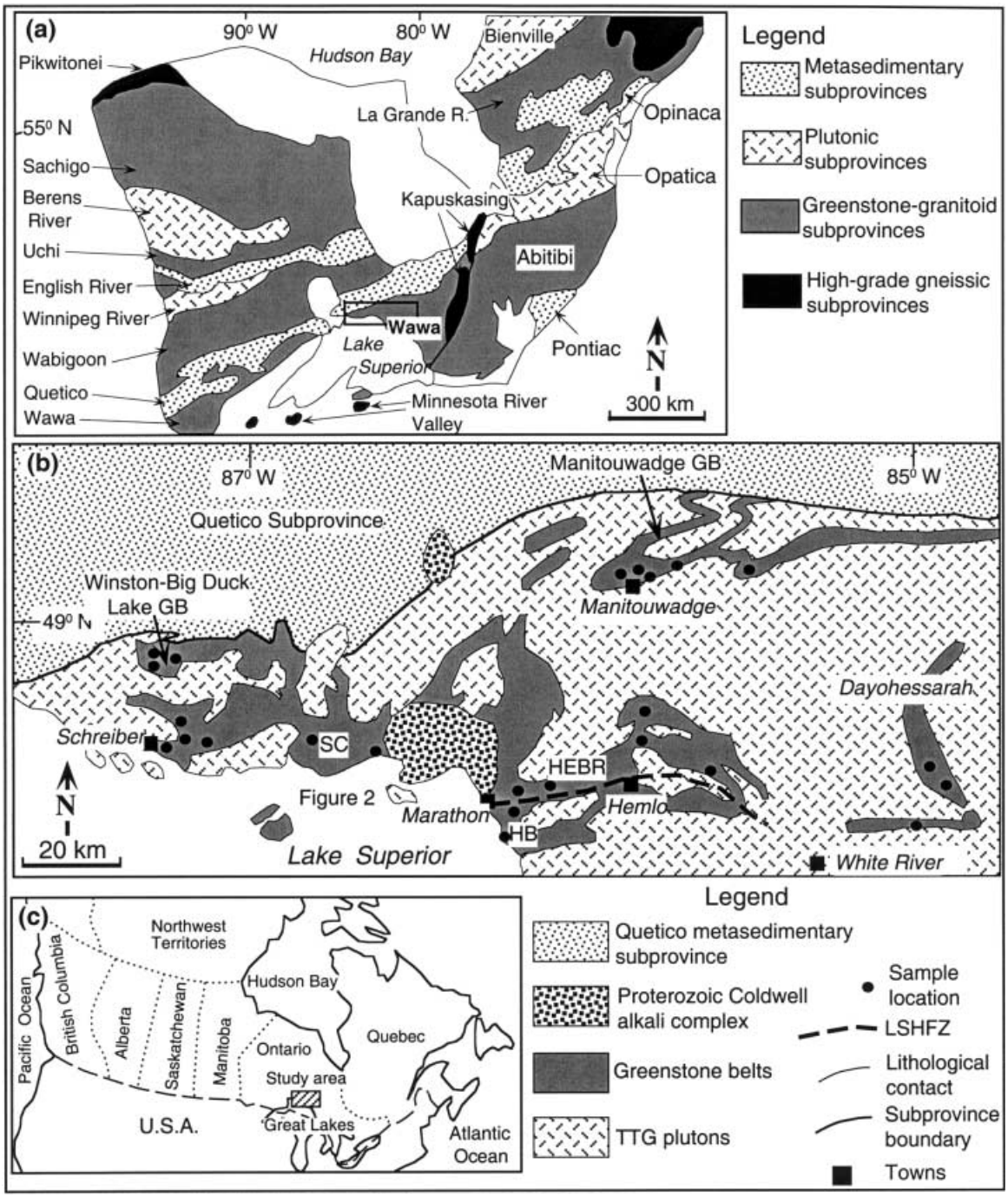

Fig. 1 **a** Generalized geological map of the Superior Province indicating the different types of subprovinces (modified after Card 1990). **b** Simplified map of the study area, showing the locations of the Schreiber-Hemlo, White River-Dayohessarah, Winston-Big Duck Lake, and Manitouwadge greenstone belts (modified after Williams et al. 1991). **c** Simplified geographic map of north central America, showing the location of the study area. *SC* Schreiber assemblage. *HEBR* Hemlo-Black River assemblage. *HB* Heron Bay assemblage

the Wawa subprovince and across the Wawa-Quetico subprovince boundary (Pan et al. 1998, and references therein). In greenschist facies rocks, chlorite and epidote are the dominant minerals in mafic rocks whereas in their amphibolite facies equivalents, hornblende and actinolitic amphiboles, plagioclase, and epidote ± garnet are predominant. Mineralogically, andesitic flows are predominantly plagioclase + hornblende ± biotite ± quartz ± chlorite. Dacites, rhyodacites, and rhyolites have quartz + alkali feldspar ± hornblende ± biotite ± muscovite phenocrysts.

Overprinting relations between different sequences of structures suggest that the Schreiber-Hemlo and White River-Dayohessarah greenstone belts underwent at least three phases of deformation. During D_1 (ca. 2695–

2685 Ma), oceanic plateau basalts and associated komatiites, arc-derived trench turbidites, and island arc volcanic sequences, including tholeiitic to calc-alkaline basalts and andesites (with the magnesian andesites, Nb-enriched basalt-andesites adakite association), were all tectonically juxtaposed as they were incorporated into an accretionary complex (Polat and Kerrich 1999). Fragmentation of these sequences resulted in broken formations and a tectonic mélange in the Schreiber assemblage, resulting in disruption of original stratigraphic relationships between different suites of volcanic rocks. D_2 (ca. 2685–2680 Ma) is consistent with an intra-arc, right-lateral transpressional deformation. Fragmentation and transposition of oceanic plateaus and island arc volcanic sequences continued during D_2. The D_1 to D_2 transition is interpreted in terms of a trenchward migration of the magmatic arc axis due to continued accretion and underplating. The D_2 intra-arc strike-slip faults may have provided conduits for rising melts from the descending slab, and they may have induced decompressional partial melting in the subarc mantle wedge to yield synkinematic ultramafic to felsic intrusions (Polat and Kerrich 1999).

The structural characteristics of the Winston-Big Duck Lake greenstone belt is relatively less studied than the Schreiber-Hemlo counterpart. Owing to poor exposure, all of the samples from this belt were obtained from drill core. Accordingly, field relationships between different suites of volcanic rocks are not well known.

Zaleski et al. (1995, 1999, and references therein) described four phases of deformation in the Manitouwadge greenstone belt of the north-central Wawa subprovince (Fig. 1b). The D_1 deformation phase is characterized by low-angle thrust faulting and folding. D_2 deformation resulted in isoclinal and sheath folds, and was accompanied by tonalite intrusion. Amphibolite facies metamorphism was broadly coeval with D_2. Deformation phase D_3 represents a regional scale transpression, producing the Manitouwadge synform. D_4 deformation is marked by outcrop-scale crenulation as well as kink band formation and map-scale open folds. Zaleski et al (1995, 1999) suggested that the D_3 dextral transpressional structures postdates the juxtaposition of the Wawa and Quetico subprovinces. As for samples of the Winston-Big Duck Lake greenstone belt, many of our samples from the Manitouwadge greenstone belt are from drill core. Thus, relationships between different volcanic rock suites are not well constrained.

In summary, there is the conjunction of tectonic juxtaposition of geochemically and geochronologically distinct volcanic and sedimentary rocks, subduction zone tectonic mélange, and regional-scale transpressional structural characteristics. Based on this conjunction, Polat et al. (1998) and Polat and Kerrich (1999) interpreted the late Archean Schreiber-Hemlo, White River-Dayohessarah, Winston-Big Duck Lake, and Manitouwadge greenstone belts as a part of continental-scale subduction-accretion complex that formed along an Archean convergent plate margin during the trenchward migration of the magmatic arc axis. In this geodynamic framework, komatiite and associated tholeiitic basalt sequences were interpreted as dismembered fragments of oceanic plateau(s). LREE-enriched and HFSE-depleted TTG plutons and associated bimodal volcanic sequences were interpreted as fragments of magmatic arcs. Siliciclastic turbidites, having positively fractionated REE patterns and HFSE depletion, were considered as trench turbidites. Volcanic rocks constitute 40–60% of the better exposed greenstone belts. Of this areal extent, all arc volcanics are 70–80%, and the ocean plateau association 20–30%. The MA, NEBA, adakite association is distributed erratically, and it is estimated to represent 5–10% of arc volcanics.

Sampling procedures and analytical methods

In this study, we present 12 published and 35 new, high-precision ICP-MS trace-element datasets (see Table 1). Samples for geochemical analyses were obtained from the least weathered outcrops of the four greenstone belts, or from core (Fig. 1). Sample locations are given as Universal Transverse Mercator (UTM) in Table 1. The samples used in this study were selected from a larger population. The subset was screened for least alteration on the criteria of preservation of igneous textures, petrographic freshness, low values of loss on ignition (LOI), and coherent chondrite-normalized (cn) REE and primitive mantle-normalized (pm) diagrams for given igneous suites. Carbonatization or silicification is less than 2% in all specimens analyzed, as determined from field and petrographic inspection. Samples were ground in an agate mill. Major elements were determined by X-ray fluorescence spectrometry [relative standard deviations (RSD) are within 5%, and totals were within $100 \pm 1\%$]. Rare earth elements, HFSE and other trace elements were analyzed by inductively coupled plasma-mass spectrometry (ICP-MS; Perkin Elmer Elan 5000) in the Department of Geological Sciences, University of Saskatchewan, using the protocol of Jenner et al. (1990), with standard additions, pure elemental standards for external calibration, BIR-1 as a reference material for mafic to intermediate rocks, and SY2 for felsic rocks. Th, Nb, Ta, Zr, Hf and the REE were determined using an Na_2O_2 sinter, and the remaining trace elements by HF-HNO_3 dissolution. The precision, at the concentration of trace elements in BIR-1 and unknowns, is generally between 2 and 10% RSD. There is excellent agreement between the recommended values for HFSE and REE in BIR-1, and the running average for these elements at the University of Saskatchewan laboratory. Samples were recalculated to 100% anhydrous for intercomparisons. Detailed descriptions of analytical procedures and values obtained for reference materials are given in Fan and Kerrich (1997).

Geochemical results

Four different volcanic rock suites are recognized from compositional characteristics (Table 1). These volcanic suites, in decreasing relative abundances, are (1) tholeiitic to calc-alkaline basalt-andesite suite, (2) magnesian andesites, (3) adakites, and (4) Nb-enriched basalts and andesites. Niobium-enriched basalts and andesites are defined on the basis of their high absolute Nb contents (> 7 ppm), and having higher Nb/Th_{pm} and Nb/La_{pm} ratios than the majority of modern oceanic

island arc basalts and andesites, plotting above the diagonal dashed line on Fig. 2.

Schreiber assemblage

Basalts and andesites in the Schreiber assemblage plot mostly in the tholeiitic field of Miyashiro (1974), and yet fractionated REE and high Zr/Y (3.2–12.2) ratios are more indicative of calc-alkaline suites (Tables 1, 2). Basalts and andesites appear to form continuous trends on diagrams of major elements versus MgO, over the range of 50–64 wt% SiO_2 and Mg-number = 0.29–0.50. However, the two define separate trends for most trace elements (Figs. 3, 4). Basalts tend to be TiO_2- and Fe_2O_3-rich, span Mg-number = 0.35–0.39, with variably Cr (14–63 ppm) and Ni (27–52 ppm) contents (Tables 1 and 2). They have variably fractionated REE and variable Nb troughs (Table 2; Fig. 5; $La/Yb_{cn} = 1.9–3.4$; $Nb/La_{pm} = 0.33–0.51$).

As a suite, the andesites to dacites define trends of smoothly decreasing TiO_2 and Fe_2O_3, increasing Th, Ce, and Zr with respect to MgO, but they have relatively uniform Nb and Yb. Accordingly, with progressive fractionation they acquire higher La/Sm_{cn} and Gd/Yb_{cn}, and pronounced Nb troughs (Fig. 5). Chromium contents of andesites are greater than in basalts (Tables 1 and 2).

Two samples are characterized by anomalously high MgO (4.8 wt%), Cr (106–147 ppm) and Ni (61–123 ppm) contents for an andesitic-dacitic range of SiO_2. These are designated as magnesian andesites, and they plot above the divide between the normal arc field and magnesian andesites (cf. McCarron and Smellie 1998; Fig. 3a). They also form trends distinct from andesites and basalts with respect to other major and trace elements. Compared to the Schreiber 'normal' andesites, MA have lesser TiO_2 at

Table 1 Major- (wt%) and trace-element (ppm) data for basalts, andesites, high-magnesian andesites (*HMA*), niobium-enriched Winston-Big Duck Lake, and Manitouwadge greenstone belts. Sample labels are *SC* Schreiber assemblage, *HB* Heron Bay assemblage, and *93* Manitouwadge belt. *n.a.* Not available

Sample no.	Basalts										Andesites		
	SC		HEBR					HB		WL	SC		
	SC95–24[a]	SC95–20	HE5	HE7	HE7–2[a]	HE8[a]	HE9[a]	HB95–15[a]	HB95–31	WL-7–2	SC95–123[a]	SC95–89	SC95–94
SiO_2	53.9	49.7	51.90	52.31	52.50	52.07	50.81	54.0	46.4	50.1	61.0	59.4	58.1
TiO_2	1.53	2.11	0.86	0.99	0.94	0.82	0.90	0.62	1.07	0.82	1.72	1.58	1.03
Al_2O_3	15.3	12.9	16.62	16.90	16.17	17.63	16.42	15.7	16.6	15.9	14.6	13.7	18.2
Fe_2O_3	12.4	18.3	10.36	9.72	9.18	8.59	11.74	9.4	16.4	11.9	8.3	14.9	6.5
MnO	0.20	0.29	0.14	0.25	0.23	0.34	0.28	0.20	0.22	0.18	0.23	0.23	0.13
MgO	3.6	4.5	5.47	5.22	5.00	4.02	4.94	4.0	5.5	6.4	2.2	2.7	2.9
CaO	9.4	9.0	11.69	10.83	12.49	10.62	11.32	11.8	11.2	11.0	5.9	4.6	6.3
K_2O	0.7	0.2	0.15	0.60	0.42	0.69	0.77	0.6	0.5	0.5	0.4	0.3	1.8
Na_2O	2.8	2.7	2.74	3.06	2.95	5.10	2.69	3.5	2.1	3.0	5.4	2.4	4.6
P_2O_5	0.20	0.30	0.06	0.13	0.12	0.10	0.14	0.22	0.10	0.17	0.23	0.21	0.39
LOI	1.3	1.1	1.80	0.75	1.90	3.10	3.40	3.7	1.2	0.7	4.9	4.4	4.0
Mg-number	0.39	0.35	0.54	0.54	0.55	0.51	0.48	0.48	0.42	0.54	0.36	0.29	0.50
Cr	63	14	200	237	198	225	208	117	362	141	137	69	136
Co	33	41						36	52	49	32	45	28
Ni	52	27	49	44	41	52	58	64	37	72	60	45	72
Rb	29	2	41	21	14	24	32	15	12	11	13	13	35
Sr	303	133	677	300	296	498	280	913	279	300	129	184	477
Cs	1.3	0.2	2.8	0.7	1.0	0.2	0.9	0.6	0.4	0.7	0.3	0.3	2.1
Ba	131	23	324	250	168	151	317	155	207	124	125	63	510
Sc	20.5	39.9	17.1	40.0	38.8	32.8	33.7	24.4	50.2	35.6	16.3	27.4	14.3
V	200	368	132	237	236	191	200	187	344	259	116	297	128
Ta	0.25	0.5	0.17	0.19	0.16	0.15	0.18	0.17	0.18	0.21	0.51	0.30	0.34
Nb	2.99	5.17	3.41	3.94	3.45	2.69	3.68	3.42	3.16	3.81	6.89	5.08	5.17
Zr	121	138	106	71	70	62	67	102	69	82	143	99	142
Hf	2.82	3.8	2.80	2.06	1.90	1.64	1.90	2.84	2.13	2.16	3.50	2.44	3.56
Th	1.00	0.79	2.26	0.92	0.82	0.56	1.06	3.51	0.81	2.44	1.47	1.00	4.61
U	0.223	0.2	0.19	0.17	0.05	0.36	0.15	0.643	0.144	0.544	0.283	0.209	0.895
Y	19.2	34.9	13.3	22.2	21.1	17.8	19.1	18.4	20.8	22.0	20.2	18.7	14.6
La	8.9	10.0	24.6	10.2	9.0	6.7	11.0	24.2	7.2	18.6	15.0	8.3	35.9
Ce	20.9	25.7	61.1	24.5	21.9	16.2	26.7	55.7	18.3	43.5	38.0	22.5	77.5
Pr	2.94	3.8	7.85	3.08	2.84	2.07	3.34	6.74	2.46	5.72	4.89	3.00	9.91
Nd	12.3	17.7	32.48	13.21	12.39	9.02	14.59	27.4	11.1	25.3	20.6	14.3	36.1
Sm	2.97	4.7	5.60	3.20	2.90	2.32	3.03	5.33	3.06	5.81	4.62	3.48	5.92
Eu	1.144	1.6	1.47	1.02	0.95	0.89	0.97	1.473	1.061	1.550	1.626	1.138	1.665
Gd	3.45	5.9	3.73	3.50	3.18	2.50	3.27	4.31	3.46	5.35	4.41	3.62	4.48
Tb	0.516	1.0	0.41	0.52	0.50	0.40	0.47	0.519	0.548	0.735	0.651	0.553	0.541
Dy	3.26	6.4	2.40	3.55	3.37	2.76	3.06	3.00	3.51	4.18	3.71	3.61	2.98
Ho	0.64	1.3	0.45	0.73	0.69	0.56	0.64	0.60	0.78	0.79	0.73	0.74	0.53
Er	1.94	3.9	1.21	2.24	2.10	1.69	1.85	1.65	2.12	2.25	1.85	1.95	1.52
Tm	0.304	0.6	0.18	0.32	0.31	0.26	0.27	0.239	0.351	0.302	0.273	0.292	0.208
Yb	1.90	3.83	1.02	1.92	1.88	1.64	1.82	1.41	2.16	1.94	1.69	1.81	1.29
Lu	0.294	0.6	0.16	0.30	0.29	0.24	0.26	0.218	0.348	0.282	0.252	0.282	0.198
East	479,055	480,451	550,578	562,140	562,140	561,861	561,688	550,504	561,625	n.a.	519,853	n.a.	478,011
North	5,410,778	5,407,962	5,395,209	5,393,095	5,393,095	5,392,966	5,392,828	5,383,965	5,392,959	n.a.	5,404,476	n.a.	5,404,590

a given value of MgO, trend to greater Th and Ce at higher MgO but to lower Nb, and have near-flat trends for Zr, Y, and Yb with MgO (Figs. 3, 4).

Hemlo-Black River (HEBR) assemblage

Magnesian andesites predominate in the population of samples from this volcanic belt, with basalts, one 'normal' andesite, and one Nb-enriched andesite. Basalts in the Hemlo-Black River assemblage are more primitive than Schreiber counterparts. Mg-number spans 0.48–0.55, and contents of Cr (200–237 ppm) and Ni (41–58 ppm) are higher. In addition, there are generally lower incompatible element contents, and low Yb with more fractionated REE ($La/Yb_{cn} = 2.9–17.3$).

Andesites are represented only by one sample in the Hemlo-Black River assemblage. It is compositionally similar to Schreiber equivalents in terms of most major elements (Tables 1, 2). It has the fractionated REE and relatively high Zr/Y (11.1) ratio of calc-alkaline suites (Fig. 5; Table 2). The majority of magnesian andesites ($SiO_2 = 57–60$ wt%; Mg-number = 0.55–0.64) plot in the HMA field on Fig. 3a, and with Schreiber MA on most major- and trace-element variation diagrams. There are some exceptions: the HEBR population includes more P-, Ce-, and Zr-rich samples, and overall this population has less fractionated LREE but more fractionated HREE (Tables 1 and 2).

Other greenstone belts

Basalts from the Winston Lake and Heron Bay assemblages are broadly compositionally akin to

basalts and andesites (*NEBA*), and adakites (aluminous rhyolites) for the 2.7 Ga Schreiber-Hemlo, White River-Dayohessarah, *HE* and *HG* Hemlo-Black River assemblage, *DH* Dayohessarah Lake area, *WR* White River area, *WL* Winston Lake assemblage, *MW*

				Magnesian andesites (MA)								
	HEBR	HB		SC		HEBR						
SC95–130	HE6–3[a]	HB96–11	HB95–29	SC95–26	SC95–43	HE1A[a]	HE6–5	HEG-8	HEG-15	HEG-20	HEG-19	HE95–29[a]
63.6	61.4	63.4	57.1	61.7	56.2	59.0	56.8	57.2	57.5	56.7	59.6	60.1
0.60	0.52	0.55	1.09	0.77	1.05	0.72	0.47	0.82	0.78	0.64	0.65	0.73
16.5	15.3	16.6	14.1	15.7	15.8	17.1	14.1	15.6	14.9	13.6	14.9	15.3
6.3	8.3	5.6	14.7	6.9	10.5	8.7	5.7	7.2	7.7	9.1	7.7	8.2
0.11	0.18	0.10	0.20	0.08	0.21	0.11	0.10	0.11	0.12	0.15	0.12	0.13
1.5	1.7	2.4	2.5	4.8	4.8	4.5	4.2	5.9	6.4	6.2	5.3	4.5
3.8	5.7	4.5	6.1	5.0	6.8	2.7	9.0	7.5	6.8	7.0	7.2	5.5
4.5	2.0	1.5	0.3	0.9	1.0	2.1	1.3	0.6	1.5	2.8	0.8	0.5
3.1	2.9	4.8	3.7	3.9	3.4	3.0	2.9	4.7	3.8	3.4	3.3	4.8
0.12	0.15	0.36	0.17	0.17	0.24	0.12	0.16	0.45	0.49	0.42	0.44	0.16
2.3	1.5	2.1	0.4	4.0	1.2	2.1	5.4	0.4	0.7	4.1	4.1	0.9
0.34	0.52	0.48	0.50	0.60	0.50	0.61	0.62	0.64	0.64	0.60	0.60	0.55
74	148	9	165	147	106	531	206	158	205	251	192	148
15		15	44	25	39			32	37	33	29	29
23	81	5	4	123	61	229	80	110	66	21	60	77
102	54	45	5	18	47	67	38	20	52	90	20	14
204	639	1,061	288	480	309	503	528	1,374	1,181	936	744	214
1.0	2.3	5.5	0.7	1.1	2.1	4.6	4.4	2.9	3.1	7.8	1.7	0.5
624	497	637	75	335	211	665	246	617	1,028	675	195	119
14.7	12.8	10.7	49.2	16.4	24.2	22.5	12.3	15.0	23.2	26.6	19.1	23.4
90	84	78	308	119	169	155	78	123	172	185	166	145
0.39	0.2	0.36	0.24	0.35	0.35	0.4	0.2	0.6	0.4	0.2	0.2	0.4
5.12	3.93	6.90	4.21	4.08	5.67	5.82	3.30	12.94	7.24	4.49	2.98	6.59
127	105	165	108	130	110	135	98	221	170	106	101	135
3.45	2.8	4.38	3.22	3.47	2.90	3.4	2.3	5.5	4.6	2.9	2.6	3.3
1.82	2.11	3.70	1.74	2.41	1.08	4.19	1.69	6.47	6.90	3.82	4.26	1.71
0.634	0.8	0.776	0.341	0.458	0.304	0.9	0.2	1.9	1.4	1.2	0.7	0.4
10.4	9.5	17.4	31.4	11.1	17.8	13.2	8.8	21.1	21.6	18.1	16.2	17.4
14.7	16.0	44.6	12.6	14.8	15.9	21.8	15.5	61.6	52.9	30.0	53.4	12.4
28.7	36.9	98.0	30.9	31.4	33.8	47.7	37.0	134.4	115.8	66.9	130.2	27.8
3.33	4.3	11.81	3.85	3.86	4.89	5.5	4.4	15.8	14.0	8.5	16.9	3.8
12.9	17.1	47.4	16.7	15.0	20.7	20.8	17.3	63.2	57.4	36.8	69.3	15.2
2.61	3.2	8.52	3.85	2.85	4.41	3.8	3.1	10.8	10.3	7.1	10.8	3.4
0.849	0.9	1.870	1.371	0.853	1.285	1.1	0.9	2.7	2.5	1.8	2.7	1.0
2.33	2.5	5.54	4.54	2.60	3.91	3.1	2.3	7.6	7.5	5.5	6.9	3.1
0.327	0.3	0.654	0.737	0.374	0.558	0.4	0.3	0.8	0.8	0.6	0.7	0.5
1.86	1.6	3.39	5.07	2.32	3.37	2.2	1.6	3.9	4.1	3.5	3.4	2.8
0.38	0.3	0.59	1.14	0.43	0.72	0.4	0.3	0.7	0.7	0.6	0.6	0.6
1.14	0.9	1.59	3.38	1.15	1.96	1.2	0.8	1.6	1.8	1.6	1.6	1.6
0.174	0.1	0.225	0.507	0.177	0.273	0.2	0.1	0.2	0.3	0.3	0.2	0.3
1.07	0.81	1.40	3.35	1.12	1.81	1.40	0.72	1.32	1.63	1.55	1.37	1.70
0.164	0.1	0.204	0.508	0.177	0.263	0.2	0.1	0.2	0.2	0.2	0.2	0.3
522,907	550,728	552,604	561,140	478,578	486,117	551,688	550728	n.a.	n.a.	n.a.	n.a.	582,828
5,404,578	5,395,163	538,958	5,392,878	5,404,405	5,429,383	5,395,273	5395163	n.a.	n.a.	n.a.	n.a.	5,413,026

Table 1 (Contd.)

Sample no.	Magnesian andesites (MA)						Nb-enriched basalts and andesites (NEBA)			
	HB	WR		MW			SC	WL		WR
	HB95–6	WR95–10	WR95–6[a]	MN9	MW95–7	MW95–15	SC95–87[a]	WL-6–2	WL-39–3	WR95–1
SiO_2	57.8	57.8	62.3	59.4	63.5	61.1	50.6	53.6	53.7	50.5
TiO_2	0.65	0.61	0.56	1.83	0.54	1.31	2.24	1.38	2.18	1.42
Al_2O_3	15.0	16.2	15.2	16.9	15.9	15.4	14.7	15.0	14.2	13.1
Fe_2O_3	8.3	8.0	6.0	6.7	6.7	6.9	16.2	11.7	13.9	16.6
MnO	0.13	0.12	0.08	0.12	0.05	0.09	0.22	0.16	0.12	0.24
MgO	6.0	5.5	3.7	3.5	3.4	3.6	5.3	5.3	4.2	5.3
CaO	6.8	5.4	5.3	5.9	6.9	7.1	7.2	8.8	7.7	9.5
K_2O	1.7	2.4	2.2	1.2	0.1	1.1	1.3	0.5	0.5	0.8
Na_2O	3.3	3.9	4.5	4.4	2.7	3.3	2.0	3.3	2.9	2.4
P_2O_5	0.25	0.10	0.19	0.08	0.12	0.12	0.27	0.27	0.52	0.14
LOI	5.9	1.0	0.8	0.1	0.4	0.6	5.2	0.5	0.6	0.9
Mg-number	0.61	0.60	0.57	0.53	0.53	0.53	0.42	0.50	0.40	0.41
Cr	353	245	166	136	110	200	22	102	14	217
Co	32	32	21	33	28	42	36	50	43	41
Ni	61	73	40	29	60	50	24	49	15	32
Rb	52	148	70	115	3	47	28	10	15	64
Sr	765	359	904	314	375	384	297	326	408	154
Cs	8.7	25.5	3.8	8.4	0.3	2.5	2.2	0.3	0.2	17.4
Ba	808	393	948	311	36	172	297	64	122	243
Sc	24.2	23.8	14.9	19.3	19.9	21.5	37.0	29.6	32.5	44.6
V	164	155	116	112	125	134	386	323	318	306
Ta	0.31	0.16	0.28	0.30	0.36	0.31	0.45	0.40	0.5	0.49
Nb	5.25	2.64	3.98	5.04	5.38	4.48	7.74	7.82	8.68	7.26
Zr	126	82	132	81	121	102	134	110	138	116
Hf	3.90	2.43	3.47	2.21	2.90	3.17	3.31	2.77	3.5	3.20
Th	2.80	1.24	5.37	2.24	2.06	2.51	1.50	1.67	2.66	2.44
U	0.659	0.284	1.148	0.540	0.472	0.473	0.326	0.472	0.6	0.501
Y	17.9	12.5	12.4	11.8	15.5	12.6	27.9	18.4	32.2	30.9
La	30.0	10.6	33.1	9.6	11.7	15.5	11.9	16.4	37.2	12.8
Ce	69.3	23.9	70.5	21.7	25.8	35.4	31.6	41.5	93.8	30.0
Pr	8.45	2.94	8.42	2.66	3.16	4.32	4.16	5.55	12.3	3.76
Nd	35.3	11.9	32.6	10.7	12.7	17.3	19.3	24.1	51.6	16.2
Sm	6.57	2.59	5.57	2.39	2.89	3.29	4.80	4.75	8.6	4.30
Eu	1.581	0.774	1.519	0.740	0.823	0.975	1.494	1.488	2.4	1.407
Gd	5.28	2.49	4.11	2.22	2.81	2.95	5.18	4.18	7.0	5.16
Tb	0.571	0.338	0.420	0.300	0.412	0.372	0.800	0.543	0.9	0.886
Dy	3.24	2.13	2.19	1.95	2.44	2.50	5.08	3.34	5.6	5.76
Ho	0.64	0.48	0.42	0.40	0.50	0.47	1.07	0.65	1.2	1.22
Er	1.63	1.35	1.11	1.18	1.42	1.32	2.95	1.84	3.3	3.46
Tm	0.269	0.215	0.147	0.190	0.211	0.201	0.431	0.281	0.5	0.535
Yb	1.44	1.32	1.09	1.24	1.38	1.47	2.60	1.71	3.24	3.47
Lu	0.242	0.196	0.140	0.200	0.201	0.211	0.379	0.261	0.5	0.515
East	552,920	642,780	638,418	n.a.	601,129	592,521	n.a.	n.a.	n.a.	633.017
North	5,389,178	5,385,759	5,385,670	n.a.	5,441,328	5,445,080	n.a.	n.a.	n.a.	5.384.871

Hemlo-Black River basalts, in terms of TiO_2 and P_2O_5 contents and other interelement systematics (Tables 1, 2).

Andesites of the Heron Bay assemblage possess similar compositions and trends to the other suites of andesites. All trace elements including Y and Yb trend higher at lower MgO. As a result, LREE become more fractionated like other andesite suites, whereas Gd/Yb_{cn} and Zr/Y ratios do not.

Three magnesian andesites from the Manitouwadge belt have a narrow compositional range, where SiO_2 = 59–63 wt%, Mg-number = 0.53, and Cr = 110–200 ppm (Tables 1, 2). These volcanics plot with, or close to, the low MgO spectrum of the Schreiber magnesian andesites, albeit to lower P and Ce but with greater Th/La_{pm} ratios (Figs. 3, 4). Magnesian andesites of the Heron Bay and White River assemblages plot with counterparts of ~6 wt% MgO, as in the larger Hemlo-Black River suite of MA (Figs. 3, 4 and 5; Tables 1, 2).

Niobium-enriched basalts and andesites (NEBA)

Niobium-enriched basalt andesites have been identified in the Schreiber assemblage (one sample), Hemlo-Black River assemblage (one sample), Winston Lake assemblage (two samples), White River-Dayohessarah belt (one sample), and Manitouwadge belt (two samples) where they coexist with magnesian andesites. Collectively, Nb spans 7–16 ppm, compared to < 2 ppm in most basalts of Phanerozoic intra-oceanic arcs (Fig. 2). Compositionally, they vary in the range 50–57 wt% SiO_2, Mg-number 0.40–0.61 and, as a group, possess generally more fractionated REE, plotting to higher Th, Nb, P_2O_5 and Y at a given value of La/Yb_{cn} than the basalts (see above, and Figs. 6, 7 and 8; Tables 1 and 2). They trend to higher Nb/Ta and Zr/Hf ratios than the basalts). Compositionally, they are similar in many respects to Cenozoic Nb-enriched basalts and andesites (Fig. 7; cf. Defant et al. 1992; Drummond et al. 1996; Sajona et al. 1996).

			Adakites							
HEBR	MW		HEBR	HB		DH	MW			
HEG-9	MN5	MW95–12	HE96–2	HB95–11	HB95–12	DH96–1	93–13	MW95–18	93–23	MW96–7
55.5	55.1	56.7	69.0	66.4	64.9	65.9	68.9	66.0	67.5	67.8
0.88	1.84	0.63	0.37	0.45	0.67	0.80	0.37	0.37	0.29	0.35
17.1	12.3	15.2	16.1	17.1	17.7	16.8	16.8	17.8	17.6	17.4
9.1	14.4	8.2	3.1	4.5	6.7	5.5	2.5	2.8	2.5	2.5
0.13	0.25	0.09	0.03	0.01	0.07	0.06	0.03	0.01	0.03	0.02
3.8	4.9	5.7	1.3	1.97	2.21	1.6	1.3	1.4	1.5	1.6
8.4	5.4	7.9	3.4	0.77	1.50	3.1	3.8	4.2	4.1	3.6
0.3	0.9	0.7	1.3	2.47	3.02	2.0	1.3	1.6	1.5	0.8
4.6	3.5	4.6	5.3	6.00	2.95	4.2	4.8	5.8	5.0	5.8
0.17	0.88	0.27	0.13	0.20	0.20	0.09	0.19	0.11	0.10	0.16
0.3	0.4	1.0	1.8	1.83	2.30	0.8	0.6	0.9	0.8	1.6
0.48	0.58	0.61	0.48	0.49	0.42	0.39	0.53	0.53	0.57	0.58
67	139	221	11	112	166	83	13	24	34	34
	37	9	13	24	27	8	12	10	10	
90	8	90	8	30	49	47	11	21	26	29
3	38	14	29	50	68	62	55	56	51	24
351	211	695	1,234	161	442	493	1,043	542	685	521
0.1	2.3	0.4	2.0	0.4	1.5	14.7	4.5	6.2	3.3	3.3
20	237	299	760	469	909	379	1,193	799	623	424
24.2	32.0	21.7	4.3	13.5	17.3	18.7	4.4	4.3	3.7	4.3
175	26	150	36	107	138	143	37	56	37	38
0.5	0.9	0.76	0.14	0.30	0.35	0.24	0.38	0.29	0.31	0.30
7.42	15.53	16.17	2.17	5.41	6.53	3.72	6.28	4.38	5.50	5.33
145	278	167	119	148	142	129	125	119	109	153
3.9	6.3	4.04	3.28	3.98	3.88	3.36	3.19	3.30	2.60	3.46
1.42	1.99	3.83	2.40	7.13	7.90	2.25	7.76	3.53	3.86	5.08
0.3	0.5	0.899	0.427	1.593	1.603	0.474	1.972	1.040	0.967	1.067
20.2	59.4	18.7	7.1	12.6	15.3	6.4	11.9	8.2	7.0	7.0
15.3	23.0	30.5	18.5	40.2	51.5	15.3	41.4	20.1	20.3	30.4
35.4	62.6	74.5	38.2	89.4	109.6	32.0	86.2	44.1	42.6	62.7
4.4	8.6	9.32	4.71	10.49	12.79	3.86	10.30	5.07	4.99	7.25
18.3	40.3	39.1	18.1	39	48	15.2	38.9	19.7	18.9	26.3
4.0	10.4	7.53	3.17	6.59	8.02	2.86	6.80	3.55	3.17	4.07
1.0	3.2	2.122	0.875	1.609	1.781	0.937	1.660	0.898	0.846	1.087
4.1	11.8	5.80	2.14	4.66	5.57	2.09	4.55	2.64	2.26	2.78
0.6	1.7	0.647	0.214	0.498	0.572	0.262	0.473	0.293	0.242	0.264
3.7	10.9	3.34	1.08	2.48	3.14	1.30	2.44	1.54	1.27	1.37
0.8	2.2	0.58	0.19	0.48	0.57	0.23	0.42	0.28	0.23	0.25
2.2	6.5	1.50	0.47	1.26	1.52	0.55	0.98	0.71	0.61	0.60
0.3	0.9	0.182	0.071	0.169	0.225	0.091	0.141	0.111	0.081	0.081
1.95	5.82	1.20	0.44	1.08	1.17	0.53	0.87	0.67	0.53	0.51
0.3	0.9	0.172	0.071	0.155	0.179	0.081	0.131	0.101	0.081	0.071
n.a.	n.a.	596,515	590,256	552,261	552,270	546,451	n.a.	587,970	n.a.	585,200
n.a.	n.a.	5,443,549	5,409,458	5,388,945	5,384,829	5,399,517	n.a.	5,443,756	n.a.	5,443,330

Adakites (Al-enriched rhyolites)

Adakites were found in all greenstone belts except the Winston Lake and Schreiber assemblages. In addition to Al_2O_3 contents of 16–18 wt%, the adakites are distinctive in (1) high La but low Yb contents resulting in extremely fractionated REE (Y = 6–15 ppm, La/Yb_{cn} = 20–43); (2) relatively high TiO_2, Fe_2O_3, MgO, Cr and Ni contents for adakites in general; (3) zero or minor Eu anomalies; and (4) pronounced troughs at Nb, Ti, Sc, and V (Fig. 6c–d; Table 1). In addition, they feature variable Nb/Ta (13–18) and Zr/Hf (35–44) ratios, spanning the respective primitive mantle values of 16 and 36 (Hofmann 1988), and both positive and negative fractionations of Zr relative to Sm (Table 1). These rocks are directly comparable to the postvolcanic, synkinematic high-Al tonalite-trondhjemite-granodorite (TTG) batholiths in the Wawa subprovince (Fig. 9; Polat et al. 1998). According to many workers, Archean high-Al TTGs and their compositionally similar Cenozoic-adakite counterparts formed by slab melting in the garnet + amphibole stability field (Lesher et al. 1986; Drummond and Defant 1990; Martin 1993; Drummond et al. 1996, and references therein).

Discussion

Tholeiitic to calc-alkaline basalt-andesite suites

Volcanic sequences in greenstone belts of the Superior Province, and Archean greenstone belts in general, are dominated by two principal associations. Tholeiitic basalt and komatiite constitute one association, and bimodal tholeiitic to calc-alkaline basalt and dacite-rhyolite the second (Condie 1981; Thurston 1990; Condie 1994). The former includes Mg- to Fe-rich tholeiitic basalts having near-flat REE patterns, with Al-depleted and/or undepleted komatiites. These flows are considered to have been erupted from mantle plumes (Arndt

and Nesbitt 1982; Cattell and Arndt 1987; Campbell and Griffiths 1992; Bickle 1993; McDonough and Ireland 1993; Xie et al. 1993; Kerrich et al. 1999a).

Bimodal volcanic sequences (Thurston et al. 1985) are generally interpreted in terms of convergent margin magmatism (Condie and Barager 1974; Condie 1994; Polat et al. 1998). A convergent margin setting for tholeiitic basalts, having the geochemical characteristics of modern primitive arc tholeiites in the western Abitibi greenstone belts, has recently been endorsed by the observation of those flows interfingering with boninite series to low-Ti tholeiites (Kerrich et al. 1998; Wyman 1999).

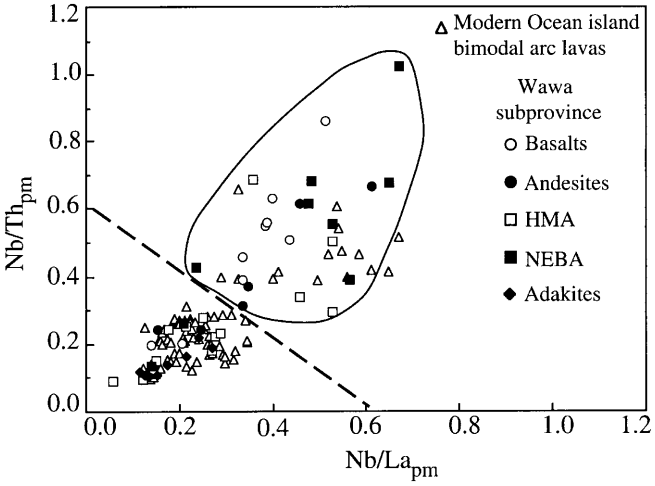

Fig. 2 Variation diagram of Nb/La_{pm} vs Nb/Th_{pm}. The majority of Phanerozoic oceanic island arc volcanic rocks plot below the diagonal *dashed line*. Basalts and andesites from the late-Archean Wawa subprovince with high Nb contents (> 7 ppm) and plotting above the *dashed line* are designated as Nb-enriched basalts and andesites (*NEBA*). Data for Phanerozoic oceanic island arc volcanic rocks are from Pearce et al. (1995) and Ewart et al. (1998)

Andesites are rare in Archean greenstone volcanic sequences (Taylor and McLennan 1985; Thurston et al. 1985; Condie 1986; Thurston 1990; Condie 1994). A continuous trend from calc-alkaline basalt, through andesite to rhyolite was described in the Marda and Welcome Well igneous complexes of the Yilgarn block by Taylor and Hallberg (1977). Ewing (1979) documented two intermediate to felsic volcanic suites at Hackett River, Northwest Territories: one is similar to modern arcs, whereas the second is an Archean high-Al type, with low Yb and fractionated HREE. Minor andesites occur in the Confederation volcanic assemblages, Uchi greenstone belt of the Superior Province, but as a whole this volcanic sequence is bimodal (Thurston and Fryer 1983).

To the authors' knowledge, significant tracts of calc-alkaline andesites have not formerly been reported from Wawa subprovince greenstone belts, or other Archean greenstone belts in general, nor specifically has the association of magnesian andesites, Nb-enriched basalt-andesites, and adakites with calc-alkaline andesites been identified before in the Wawa subprovince. One other occurrence of this association has been documented in the 2.7 Ga Uchi greenstone belt of the northern Superior Province (Hollings and Kerrich 2000).

Table 2 Summary of significant compositional and element ratios for basalts, andesites, magnesian andesites (*MA*), Nb-enriched basalts and andesites (*NEBA*), and adakites of the Wawa subprovince greenstone belts

	Basalts	Andesites	MA	NEBA	Adakites
SiO_2 (wt%)	46–54	57–63	56–64	50–57	64–69
MgO	3.6–6.4	1.5–2.9	3.4–6.4	3.8–5.7	1.3–2.2
TiO_2	0.6–2.1	0.5–1.7	0.47–1.83	0.63–2.24	0.29–0.80
Fe_2O_3	8.6–18.3	5.6–14.9	5.7–10.5	8.2–16.6	2.5–6.7
Mg-number	0.35–0.55	0.29–0.52	0.50–0.64	0.40–0.61	0.39–0.58
Cr (ppm)	14–362	9–165	106–531	14–221	11–166
Ni	27–72	4.0–81	21–229	8.5–90.1	8.0–49.0
Sc	17–50	10.7–49.2	12.3–26.6	24.2–44.6	4.3–18.7
Zr	62–138	99–165	81–221	110–278	109–153
Nb	2.7–5.2	3.9–6.9	2.6–12.9	7.3–16.2	2.17–6.53
Th	0.56–3.51	1.00–4.60	1.08–6.90	1.42–3.83	2.40–7.90
La	6.7–24.6	8.3–44.6	9.6–61.6	11.9–37.2	15.3–51.5
Y	13.3–35.0	9.5–31.4	8.8–21.6	18.4–59.4	6.4–15.3
Yb	1.0–3.8	0.81–3.35	0.72–1.81	1.20–5.82	0.44–1.17
La/Sm_{cn}	1.37–2.93	1.54–3.92	2.34–3.83	1.42–2.79	3.4–4.8
La/Yb_{cn}	1.88–17.31	2.70–22.88	5.26–27.9	2.65–18.19	20.5–42.9
Gd/Yb_{cn}	1.28–3.07	1.14–3.32	1.50–4.87	1.25–4.05	2.3–4.6
Zr/Y	3.2–7.9	3.43–12.18	5.86–11.68	3.76–8.91	9.3–21.7
Zr/Hf	32.6–43.0	33.4–40.8	32.1–42.6	36.3–44.3	36.1–44.1
Nb/Ta	11.4–21.6	13.2–19.3	11.6–19.4	14.9–21.3	14.9–18.7
Ti/Zr	37–92	20–96	26–135	22.4–100.2	13.9–36.9
Zr/Sm_{pm}	0.56–1.63	0.77–1.94	0.37–1.81	0.64–1.46	0.71–1.79
Al_2O_3/TiO_2	6.1–25.1	8.5–30.1	9.2–30.1	6.6–24.1	21–61
Nb/La_{pm}	0.14–0.51	0.14–0.61	0.06–0.53	0.23–0.67	0.12–0.27
Th/La_{pm}	0.59–1.1	0.63–1.04	0.51–1.77	0.54–1.43	0.98–1.44
Nb/Th_{pm}	0.13–0.86	0.15–0.67	0.09–0.69	0.39–1.03	0.10–0.22

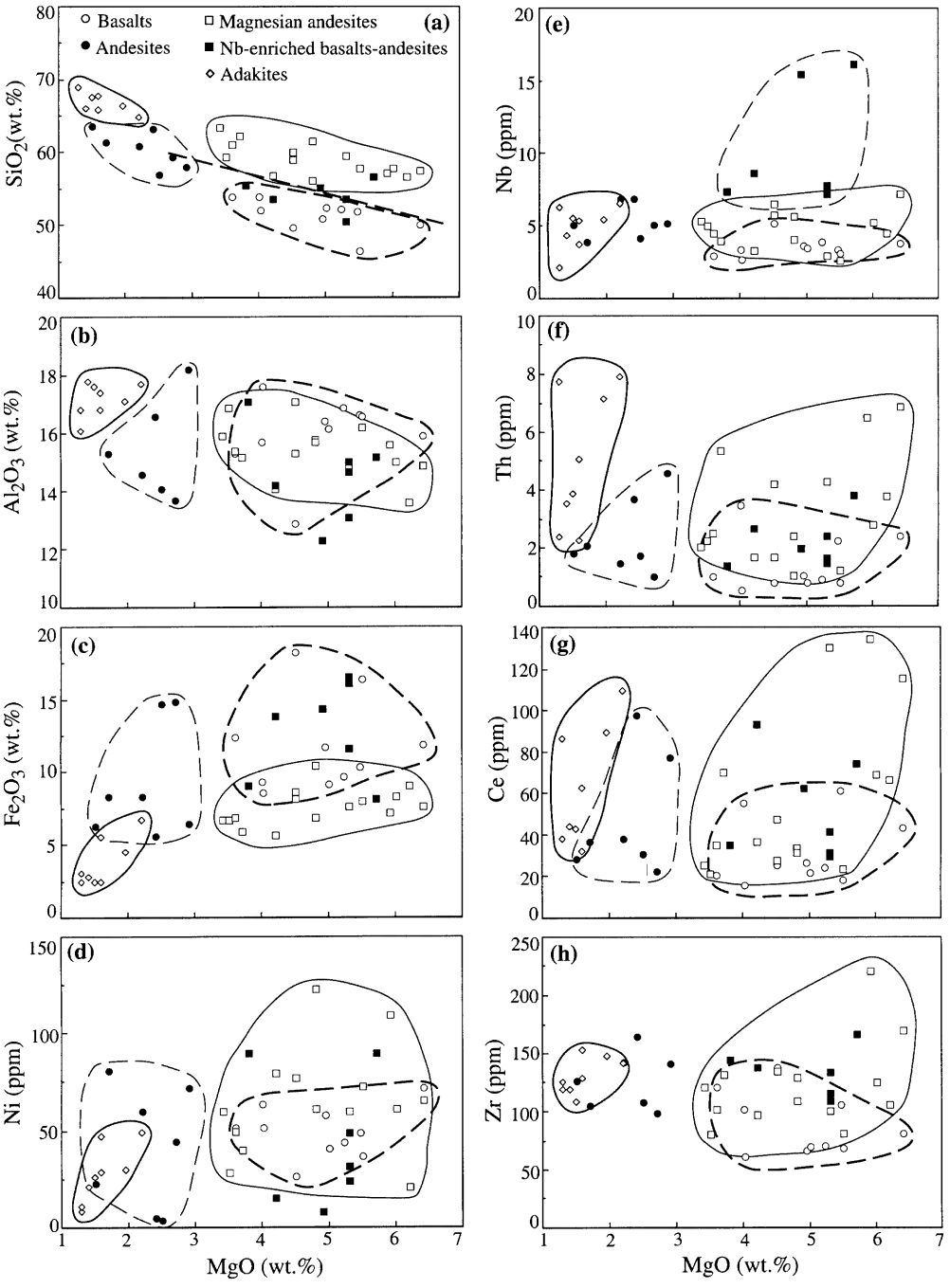

Fig. 3a–h Variation diagrams of MgO vs SiO_2, Al_2O_3, Fe_2O_3, Ni, Th, Ce, and Zr. *Dashed line* in **a** after McCarron and Smellie (1998). Outlier samples SC95–130 and HEG-8 were not plotted in **b** and **e**, respectively

Fractionation-mixing trends

Basalts and andesite suites from the Schreiber and Hemlo-Black River assemblages plot predominantly in the tholeiite field of Miyashiro (1974). However, both suites show trends of decreasing TiO_2, Fe_2O_3, and Zr with increasing fractionation as monitored by MgO, and increase of La/Yb_{cn} and Zr/Y ratios characteristic of calc-alkaline fractionation trends. As a corollary, there are no trends of decreasing Al_2O_3 with development of negative Eu anomalies as documented for tholeiitic basalts of the Blake River group of the Abitibi greenstone belt (Laflèche et al. 1992).

In comparing the Schreiber and Hemlo-Black River basalts and andesites, both basalt suites show generally decreasing to flat trends of P_2O_5, Th, Ce, Zr, and Yb contents to lower MgO. The former trend to slightly higher whereas the latter trend to sharply lower La/Sm_{cn}, Gd/Yb_{cn}, and Zr/Y ratios (Fig. 5; Table 1). In contrast, andesites of the Schreiber assemblage fractionate to greater P_2O_5, Th, Ce, and Zr but lesser Yb (Table 1). The Hemlo-Black River andesite show the same relationship of these elements with respect to MgO (P_2O_5 and Zr excepted; Fig. 5).

Indices of REE fractionation and Zr/Y ratios collectively increase with fractionation in the andesites.

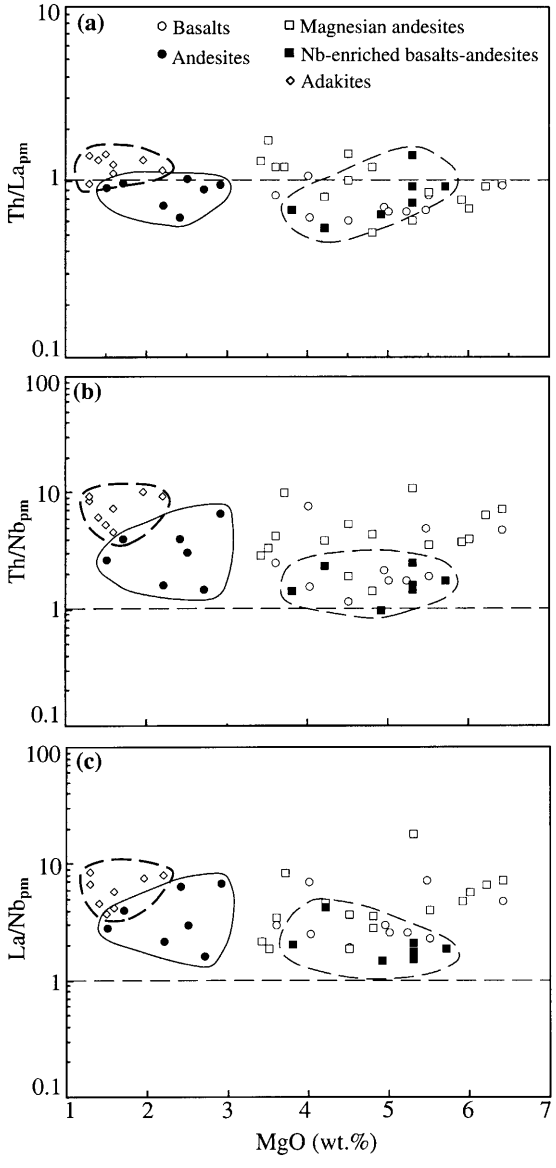

Fig. 4 Variation diagrams of MgO vs Th/La$_{pm}$, Th/Nb$_{pm}$, and La/Nb$_{pm}$. Primitive mantle-normalization values are from Hofmann (1988)

All basalts and andesites are characterized by decrease of Nb and Ti with evolution, likely due in part to fractional crystallization of a Ti-bearing phase. Based on the differences in compositional trends, andesites and basalts in each of the Schreiber and Hemlo-Black River assemblages represent different magma series with distinct fractionation trends. Within some of the basalt and andesite suites it is evident that the compositional variation does not conform to typical calc-alkaline differentiation trends. Rare earth element contents and La/Yb$_{cn}$ ratios do not systematically covary with indices of fractionation such as SiO_2 or MgO in a manner consistent with amphibole and magnetite crystal fractionation (cf. Hochstaedter et al. 1996).

In both suites of basalts and andesites, those with the greatest LREE contents also feature high La/Yb$_{cn}$ ratios, low Yb, deep Nb and Ti troughs, pronounced depletion of Sc and V relative to REE, and generally low Cr, Co, and Ni contents. These are all compositional characteristics of adakites, yet these samples are too low in SiO_2, MgO, and Fe_2O_3 to be adakites.

Accordingly, we interpret the complex spectrum of basalt and andesite compositions in terms of some combination of calc-alkaline fractionation trends, with hybridization (metasomatism) of the source of the basalts and andesites by aluminous adakite liquids. Such mixing trends between basalt and adakite endmembers are evident on Fig. 9. According to Thurston and Fryer (1983), complex trends in andesites of the Confederation-area Uchi greenstone belt could be accounted for by hybridization of tholeiitic basalts with trondhjemitic liquids (member of the high-Al TTG suite), and Laflèche et al. (1992) proposed a similar mechanism for the generation of andesites in the Blake River Group, Abitibi belt.

Petrogenesis of Al-enriched adakites and magnesian andesites

The adakites share the fractionated REE and low Yb contents of coeval tonalite-trondhjemite-granodiorite to intrusive suites in the Wawa greenstone belts. They plot with Archean TTG in general (Fig. 9; Polat et al. 1998), and are compositionally akin to Cenozoic adakites (Fig. 7). Drummond et al. (1996) distinguished two types of high-Al tonalite-trondhjemite-dacite (TTD) suite. Both are characterized by >15 wt% Al_2O_3 at 70 wt% SiO_2, and have low Y, Yb and Sc with high Sr contents and Sr/Y, La/Yb$_{cn}$ and Zr/Sm ratios. The second type, which comprises Cenozoic adakites and the Archean high-Al tonalite trondhjemite granodiorite (TTG) suite trend to more extreme compositional values and ratios. According to Drummond et al. (1996), the former type is considered to represent slab melting with a garnet-hornblende-clinopyroxene residue, whereas the latter has a garnet-amphibole to eclogite residue. Cenozoic adakites have $Y<16$ ppm and mostly 5–10 ppm, La/Sm$_{cn}$ mostly in the range 20–200 (Drummond and Defant 1990; Defant and Drummond 1990; Defant et al. 1992). The adakite-like Al-enriched dacite-rhyolites of this study conform to these compositional criteria.

Removal of subaluminous hornblende and garnet, either as restite or during early high-pressure crystallization, produce the high-Al, low-Yb compositions. High Zr/Sm ratios stem from the incompatibility of Zr in residual amphibole (Drummond et al. 1996, and references therein). Trends to high MgO, Cr, Co, and Ni can be accounted for by interaction between siliceous slab melts and the peridotitic subarc mantle wedge, and this is also responsible for variable SiO_2 contents (cf. Martin 1993; Tables 1 and 2).

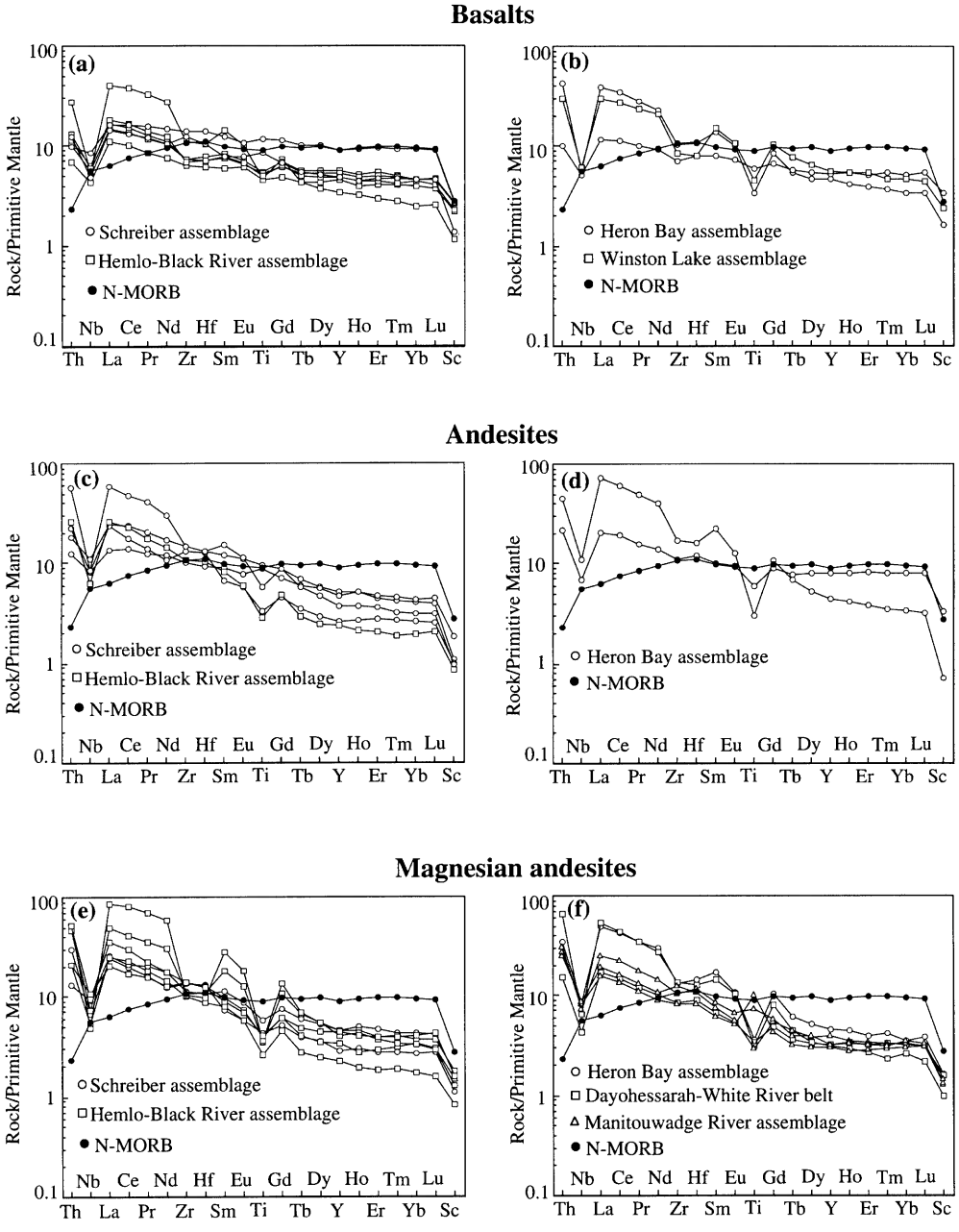

Fig. 5 Primitive mantle-normalized trace-element diagrams for basalt, andesites, and magnesian andesites. N-MORB and primitive mantle normalization values as for Fig. 4

Magnesian andesites

There are continuous trends on many of the variation diagrams from basalts and andesites, through basalts and andesites mixed with adakite-type liquids to magnesian andesites and end-member adakites (Figs. 3, 4 and 9). Models for the generation of high-magnesian andesites have recently been reviewed by Kelemen (1995). They likely form by progressive hybridization of adakite liquids with peridotite mantle wedge, which accounts for their 'normal' character of high MgO, Cr, Ni, Th and Ce contents compared with fractionated REE, low Yb, and pronounced negative Nb and Ti anomalies (Fig. 5e–f; Yogodzinski et al. 1995).

Nb-enriched basalts and andesites

High-Nb basalts are defined by Nb contents greater than 20 ppm, whereas Nb-enriched basalts have variably lower contents (6–20 ppm) but are considerably greater than typical for intra-oceanic arc basalts where Nb may be less than 2 ppm (Sajona et al. 1996; Taylor and Nesbitt 1998). Compositions of Nb-enriched basalt-adakite associations have been compiled by Sajona et al (1996; see also Drummond et al. 1996, and Sajona et al. 1993). Niobium-enriched lavas of this study differ from E-MORB-type-enriched tholeiitic basalts with broadly similar primitive mantle-normalized patterns (Hofmann 1988; Sun and McDonough 1989), in having more fractionated REE, extending to high Nb and Ti but

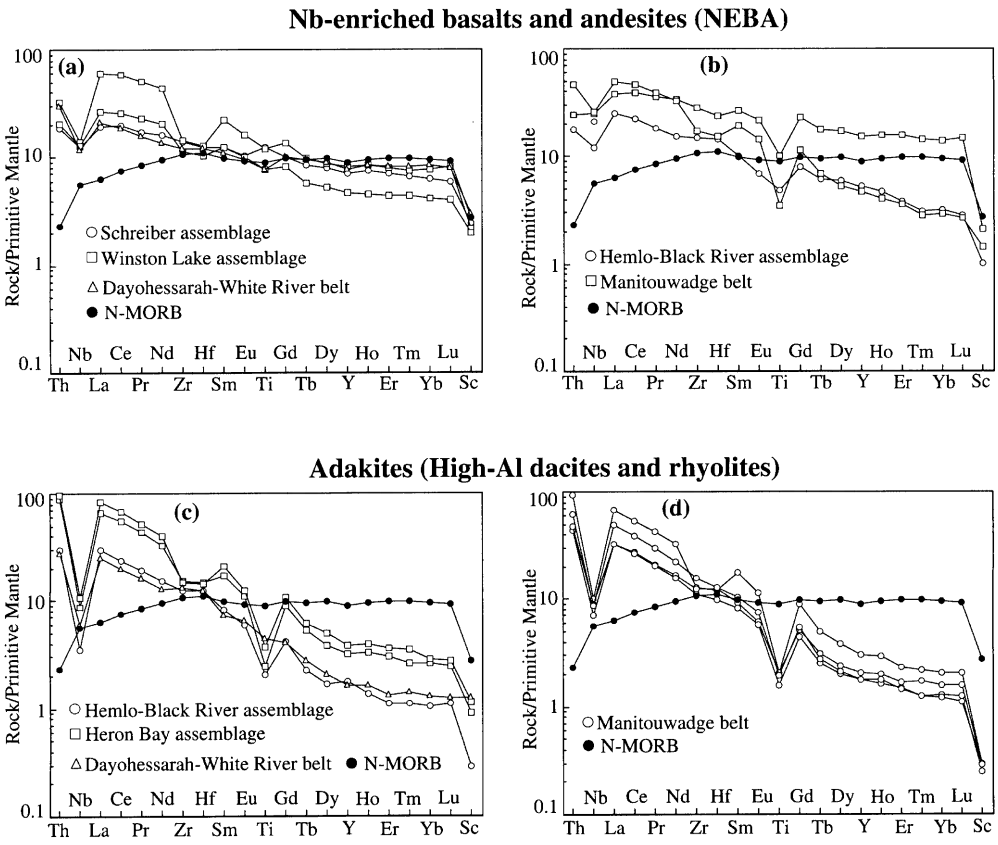

Fig. 6 Primitive mantle-normalized trace-element diagrams for Nb-enriched basalts and andesites and adakites (aluminous dacites and rhyolites). N-MORB and primitive mantle normalization values as for Fig. 4

lower Yb contents, and to greater Nb/Ta and Zr/Hf but lower Zr/Sm ratios (Table 1). They also have systematically lower Ni, Cr and Co but higher SiO_2 contents characteristic of Phanerozoic Nb-enriched basalts, in contrast to HMA (Sajona et al. 1996).

Several studies have addressed the spatial association of Phanerozoic Nb-enriched basalts and andesites with adakites (Kepezhinskas et al. 1995). There may also be 'normal' arc volcanics and magnesian andesites present with this association. For example, in Panama and Costa Rica older island volcanics are succeeded by a younger adakite-Nb-enriched basalt association (Defant et al. 1992). In the Zamboanga arc, Philippines, there is a suite of lavas ranging from high-Nb basalts to adakites (Sajona et al. 1996). Yogodzinski et al. (1995) describe magnesian andesites associated with calc-alkaline suites in the Piip volcano, western Aleutians.

According to Sajona et al. (1996, and references therein), the Nb-enriched basalt adakite association results from the following events: (1) adakite liquids form by slab melting during shallow subduction of young, hot oceanic lithosphere; (2) these liquids may erupt, or alternatively react with subarc mantle peridotites; the resultant liquid is an adak-type HMA or, if reaction proceeds further, a Piip-type HMA (Fig. 9; transitional adakites of Drummond et al. 1996, and references therein); (3) the mantle is metasomatically altered by the adakite liquids to an amphibole and ilmenite, or amphibole and Fe-rich orthopyroxene assemblage that scavenges HFSE from the liquid; and (4) induced convection in the subarc mantle drags the metasomatically altered peridotite to depths where it melts, generating NEB liquids (Sajona et al. 1993; Kepezhinskas et al. 1995, 1996; Sajona et al. 1996). Alternatively, Yogodzinski et al. (1995) invoke breakdown of phases in the slab itself to account for their rare NEB. Niobium-enriched basalts and andesites of this study most closely resemble the CA group of Sajona et al. (1996), which features high Nb contents with small Nb troughs in primitive mantle-normalized diagrams (Figs. 2, 6).

Implications for geodynamic setting and continental growth

In general, the geochemical characteristics of modern volcanic rocks from different tectonic settings are distinct in terms of their large ion lithophile element (LILE), rare earth element (REE), and high field strength element (HFSE) systematics (Pearce and Cann 1973; Pearce 1982; Sun and McDonough 1989; Pearce and Peate 1995). Similar geochemical behavior should also be expected in Archean volcanic rocks, given that certain groups of elements will behave consistently for a particular petrogenetic process throughout Earth's history. The geochemical characteristics of magmatism in modern subduction zones is controlled mainly by (1) the age of the subducting plate (e.g., young versus old); (2) the nature of the overriding plate (e.g., continental ver-

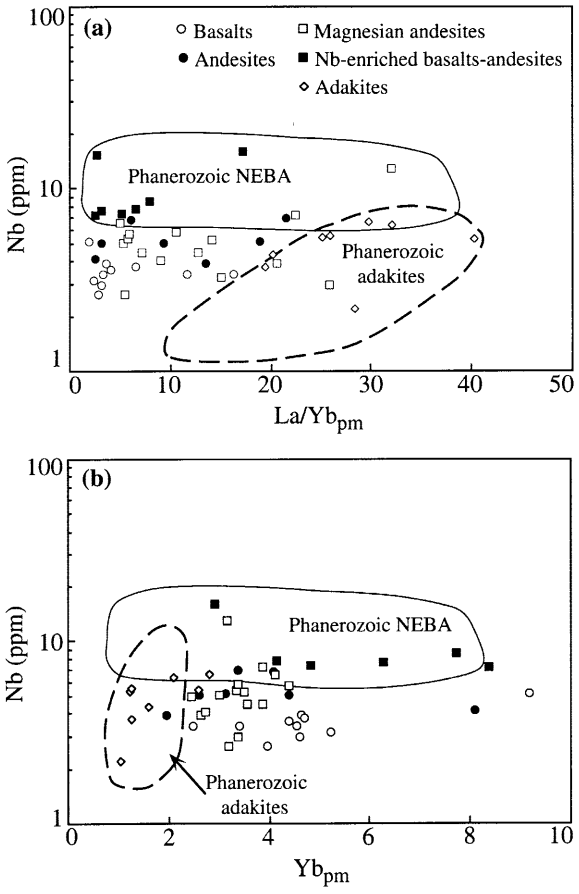

Fig. 7 Variation diagrams of **a** La/Yb_{pm} vs Nb, and **b** Yb_{pm} vs Nb. Fields for Phanerozoic volcanic rocks are from Defant et al. (1992), Stern and Kilian (1996), Sajona et al. (1996), and McCarron and Smellie (1998). Primitive mantle normalization values as for Fig. 4. Outlier sample MN5 was left out in **b**

sus oceanic); (3) the presence or absence of sediment subduction; (4) the subduction velocity (e.g., slow versus rapid); (5) the angle of subduction (e.g., shallow versus steep); (6) the convergence angle (e.g., orthogonal versus oblique); (7) the previous history of the subarc mantle wedge; and (8) the presence or absence of a backarc basin opening (Wilson 1989; Drummond and Defant 1990; Pearce and Peate 1995; Pearce et al. 1999).

Based on the close geochemical and structural similarities between Wawa greenstone belts and specific Phanerozoic subduction-accretion complexes, the late-Archean Wawa greenstone belts have been interpreted as remnants of oceanic plateaus, island arcs, and trench turbidites which were tectonically assembled in a large subduction-accretion complex (Polat et al. 1998; Polat and Kerrich 1999). In the Schreiber-Hemlo greenstone belt, imbricated lithotectonic assemblages are often disrupted by synaccretion strike-slip faults, suggesting that strike-slip faulting was an important aspect of greenstone belt evolution (Polat et al. 1998). According to Polat and Kerrich (1999), D_2 strike-slip faults in the Schreiber-Hemlo magmatic arc may have induced decompressional partial melting in the subarc mantle wedge, and provided conduits for melts from both the slab and wedge.

It appears that many modern magnesian andesites, Nb-enriched basalts and andesites, and adakites are closely associated with the subduction of young, hot oceanic slabs in, for example, the Philippines (Sajona et al. 1993, 1996), southern Andes (Stern and Kilian 1996), Central America (Defant et al. 1992), and western Aleutian Islands (Yogodzinski et al. 1994, 1995). Similarly, subduction of young, hot oceanic slabs may have been responsible for the generation and association of HMA, NEBA, and adakites in late-Archean Wawa subprovince greenstone belts.

In this framework, high-Al TTG plutons, tholeiitic to calc-alkaline bimodal volcanic rocks, and ultramafic to felsic dikes and sills, with positively fractionated REE patterns and negative Nb and Ti anomalies, are interpreted as magmatic arc associations. Given a number of lines of evidence for higher geothermal gradients in the Archean mantle, the origin of high-Al, high La/Yb_{cn} TTGs in Archean greenstone-granitoid terranes has been attributed to the melting of young, hot oceanic slabs at subduction zones (Martin 1986, 1993; Drummond et al. 1996, and references therein).

Although the rate of Archean continental growth and recycling is a matter of geological debate (Taylor and McLennan 1985, 1995; Sylvester et al. 1997; Kerrich et al. 1999b, and references therein), it is generally accepted that Archean continental crust grew by accretionary and magmatic processes taking place at convergent plate boundaries (Kusky and Polat 1999). Many continental growth models suggest that about 70% of the present-day continental crust formed by the end of the Archean (Taylor and McLennan 1995; Hofmann 1997, and references therein). Recent studies suggest that the accretion of mantle plume-derived oceanic plateaus at convergent plate margins may have played an important role throughout Earth's history in the growth of the continental crust (Stein and Hofmann 1994; Condie 1998; Puchtel et al. 1998; Kerrich et al. 1999a, 1999b, and references therein).

The average geochemical composition of the bulk continental crust is andesitic (Taylor and McLennan 1985, 1995; Rudnick 1995), and is not consistent with either arcs or accretion of oceanic plateaus alone. Similarly, accretion of oceanic island arcs with or without an oceanic plateau basement is insufficient to account for the geochemical composition of the continental crust (Rudnick 1995). For these reasons, postaccretionary geological processes, including granitoid intrusion, subduction erosion, intracrustal differentiation, lithospheric delamination, and decoupling of plateaus from overlying island arcs, taking place at convergent margins have been invoked to explain the andesitic bulk composition of the continental crust (Taylor and McLennan 1995; Albarède 1998; Polat and Kerrich 2000).

In the Wawa subprovince, there is a spatial and temporal association of magnesian andesites which are associated with tholeiitic to calc-alkaline basalts, 'nor-

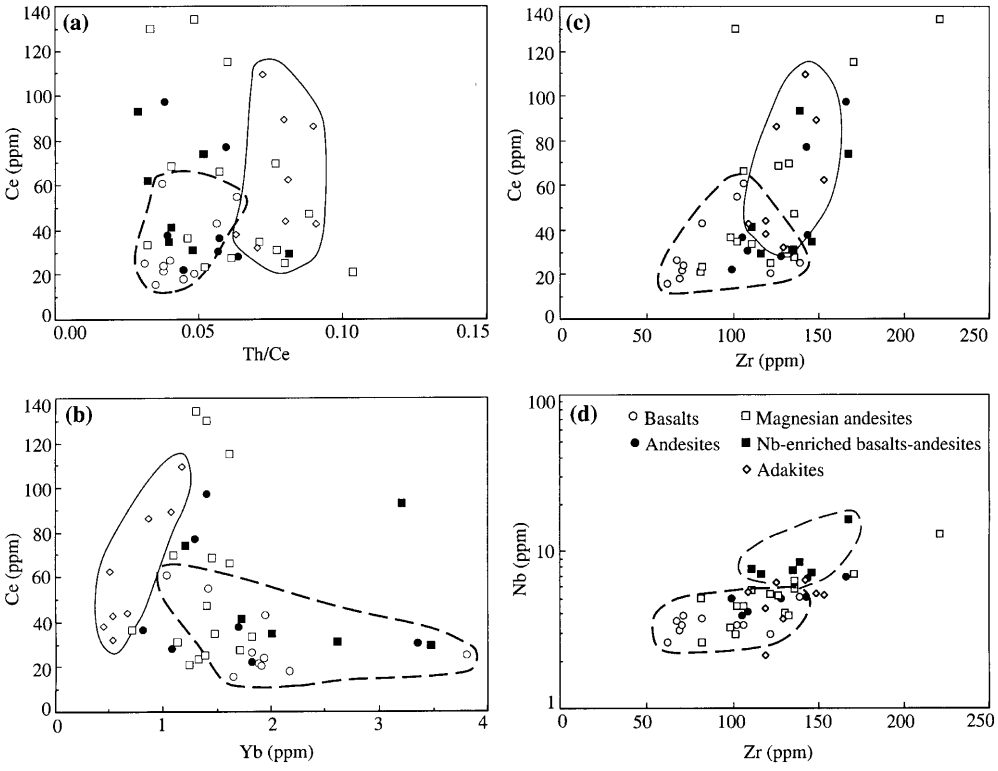

Fig. 8 Variation diagrams of **a–b** Th/Ce and Yb vs Ce, and **c–d** Zr vs Ce and Nb. Outlier sample HEG-8 was left out in **c** and **d**

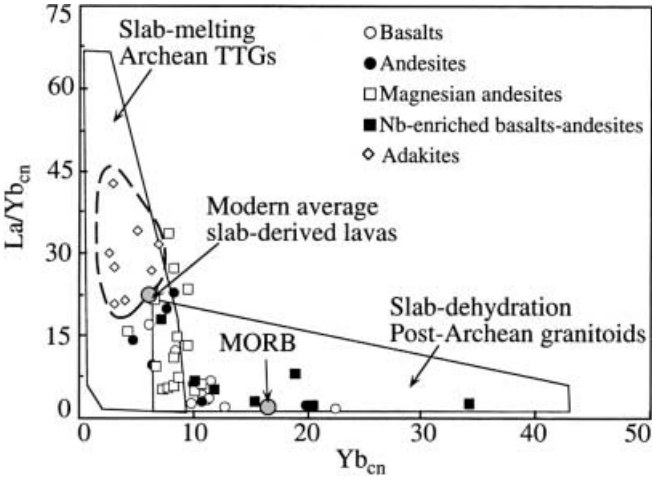

Fig. 9 Variation diagram of Yb_{cn} vs La/Yb_{cn}. Fields are after Martin (1986, 1993). Chondrite normalization values are from Sun and McDonough (1989)

mal' andesites, Nb-enriched basalts and andesites, and adakites with TTG-like geochemical characteristics, suggesting a genetic link between them. It has been proposed that in the Archean high heat flow, rapid mantle convection and subduction of young, hotter oceanic slabs provided optimized conditions for the transformation of slabs into continental protoliths via partial melting under garnet amphibolite to eclogite conditions (Drummond and Defant 1990; Defant and Drummond 1990), resulting in generation of TTGs, sanukitoids, and magnesian basalts to andesites at Archean subduction zones (Martin 1993; Drummond et al. 1996).

Based on compositional similarities between orogenic magnesian andesites and the continental crust, Kelemen (1995) suggested that magnesian andesite protoliths, forming at subduction zones with higher geothermal gradient, may constitute a substantial amount of the continental crust. However, HMA are rare in both the Archean and Phanerozoic rock records. They constitute volumetrically less than a few percent of the exposed Wawa subprovince crust. Their significance is a record of the highly prescribed plate-tectonic setting in which they form. Rather, the Mg, Ni deficit of the andesite model for growth of continental crust is better accounted for by incorporation of the more abundant ocean plateau basalt-komatiite association into arcs (Rudnick 1995; Polat and Kerrich 2000).

Acknowledgments We thank D.A. Wyman and P. Hollings for thoughtful discussion on Archean volcanism. J. Jain and B. Morgan provided assistance with ICP-MS. Comprehensive critiques by M. Defant and two anonymous reviewers have resulted in significant improvements to the paper. This paper was written when A. Polat was a recipient of Alexander von Humboldt fellowship. The research was funded through an NSERC operating grant to R. Kerrich, and as part of an NSERC-IOR to MITEC (CAMIRO) 93EOR.

References

Albarède F (1998) The growth of continental crust. Tectonophysics 296:1–14

Arndt NT, Nesbitt RW (1982) Geochemistry of Munro Township basalts. In: Arndt NT, Nisbet EG (eds) Komatiites. Allen and Unwin, London, pp 309–329

Bickle MJ (1993) Plume origin for komatiites. Nature 365:390–391

Campbell IH, Griffiths RW (1992) The changing nature of mantle hot spots through time: implications for the chemical evolution of the mantle. J Geol 92:497–523
Card KD (1990) A review of the Superior Province of the Canadian Shield, a product of Archean accretion. Precambrian Res 48:99–156
Card KD, Ciesielski A (1986) DNAG No. 1. Subdivision of the Superior Province of the Canadian Shield. Geosci Can 13:5–13
Cattel A, Arndt NT (1987) Low- and high-aluminum komatiites from a late Archean sequence, Newton township, Ontario. Contrib Mineral Petrol 97:218–227
Condie KC (1981) Archaen greenstone belts. Elsevier, Amsterdam
Condie KC (1986) Origin and early growth rate of continents. Precam Res 32:261–278
Condie KC (1994) Greenstones through time. In: Condie KC (ed) Archaen crustal evolution. Elsevier, Amsterdam, pp 85–121
Condie KC (1998) Episodic continental growth and supercontinents: a mantle avalanche connection? Earth Planet Sci Lett 163:97–108
Condie KC, Barager WRA (1974) Rare-earth element distributions in volcanic rocks from Archean greenstone belts. Contrib Mineral Petrol 45:237–246
Defant MJ, Drummond MS (1990) Derivation of some modern arc magmas by meting of young subducted oceanic lithosphere. Nature 347:662–665
Defant MJ, Jackson TE, Drummond MS, De Boher JZ, Bellon H, Feigenson MD, Maury RC, Stewart RH (1992) The geochemistry of young volcanism throughout western Panama and southeastern Costa Rica: an overview. J Geol Soc Lond 149:569–579
Drummond MS, Defant MJ (1990) A model for trondhjemite-tonalite-dacite genesis and crustal growth via slab melting: Archean to modern comparisons. J Geophys Res 95:21503–21521
Drummond MS, Defant MJ, Kepezhinskas PK (1996) Petrogenesis of slab-derived trondhjemite-tonalite-dacite/adakite magmas. Trans R Soc Edinb Earth Sci 87:205–215
Ewart A, Collerson KD, Regelous M, Wendt JI, Niu Y (1998) Geochemical evolution within the Tonga-Kermadec-Lau arc-back-arc system: the role of varying mantle wedge composition in space and time. J Petrol 29:331–368
Ewing TE (1979) Two calc-alkaline volcanic trends in the Archean: trace element evidence. Contrib Mineral Petrol 70:1–7
Fan J, Kerrich R (1997) Geochemical characteristics of Al-depleted and undepleted komatiites and HREE-enriched tholeiites, western Abitibi greenstone belt: variable HFSE/REE systematics in a heterogeneous mantle plume. Geochim Cosmochim Acta 61:4723–4744
Hochstaedter AG, Kepezhinskas PK, Defant MJ, Drummond MS, Koloskov A (1996) Insights into the volcanic arc mantle wedge from magnesian lavas from the Kamchatka arc. J Geophys Res 101:697–712
Hofmann AW (1988) Chemical differentiation of the Earth: the relationship between mantle continental crust and oceanic crust. Earth Planet Sci Lett 90:297–314
Hofmann AW (1997) Early evolution of continents. Science 275:498–499
Hollings P, Kerrich R (2000) An Archean arc basalt-Nb-enriched basalt-adakite association: The 2.7 Ga Confederation assemblage of the Birch-Uchi greenstone belt, Superior Province. Contrib Mineral Petrol 139:208–226
Jenner GA, Longerich HP, Jackson SE, Fryer BJ (1990) ICP-MS – a powerful tool for high precision trace element analysis in earth sciences: evidence from analysis of selected U.S.G.S. reference samples. Chem Geol 83:133–148
Kelemen PB (1995) Genesis of high Mg# andesites and the continental crust. Contrib Mineral Petrol 120:1–19
Kepezhinskas P, Defant MJ, Drummond MS (1995) Na-metasomatism in the island arc mantle by slab melt-peridotite interaction: Evidence from mantle xenoliths in the North Kamchatka arc. J Petrol 36:1505–1527
Kepezhinskas P, Defant MJ, Drummond MS (1996) Progressive enrichment of island arc mantle by melt-peridotite interaction inferred from Kamchatka xenoliths. Geochim Cosmochim Acta 60:1217–1229
Kerrich R, Wyman D, Fan J, Bleeker W (1998) Boninite series: low Ti-tholeiite association from 2.7 Ga Abitibi greenstone belt. Earth Planet Sci Lett 164:303–316
Kerrich R, Polat A, Wyman DA, Hollings P (1999a) Trace element systematics of Mg- to Fe-tholeiitic basalt suites of the Superior Province: implications for Archean mantle reservoirs and greenstone belt genesis. Lithos 46:163–187
Kerrich R, Wyman D, Hollings P, Polat A (1999b) Variability of Nb/U and Th/La in 3.0 to 2.7 Ga Superior Province ocean plateau basalts: implications for the timing of continental growth and lithosphere recycling. Earth Planet Sci Lett 168:101–115
Kusky TM, Polat A (1999) Growth of granite-greenstone terranes at convergent margins, and stabilization of Archean cratons. Tectonophysics 305:43–73
Laflèche MR, Dupuy C, Dostal J (1992) Tholeiitic volcanic rocks of the late Archean Blake River Group, southern Abitibi greenstone belt: origin and geodynamic implications. Can J Earth Sci 29:1448–1458
Lesher CM, Goodwin AM, Campbell IH, Gorton MP (1986) Trace-element geochemistry of ore associated with barren, felsic metavolcanic rocks in the Superior Province. Can J Earth Sci 23:222–237
Martin H (1986) Effect of steeper Archean geothermal gradient on geochemistry of subduction zone magmas. Geology 14:753–756
Martin H (1993) The mechanisms of petrogenesis of the Archean continental crust – comparison with modern processes. Lithos 30:373–388
McCarron JJ, Smellie JL (1998) Tectonic implications of fore-arc magmatism and generation of high-magnesian andesites: Alexander Island, Antarctica. J Geol Soc Lond 155:269–280
McDonough WF, Ireland TR (1993) Intra-plate origin of komatiites inferred from trace element in glass inclusions. Nature 365:432–434
Miyashiro A (1974) Volcanic rock series in island arcs and active continental margins. Am J Sci 274:321–355
Muir TL (1997) Hemlo gold deposit area. In: Precambrian geology. Ontario Geol Surv Rep 289
Pan Y, Fleet ME, Heaman L (1998) Thermo-tectonic evolution of an Archaen accretionary complex: U-Pb geochronological constraints on granulites from the Quetico subprovince, Ontario, Canada. Precambrian Res 92:117–128
Pearce JA (1982) Trace element characteristics of lavas from destructive plate boundaries. In: Thorpe RS (ed.) Orogenic andesites and related rocks. Wiley, Chichester, pp 525–548
Pearce JA, Cann JR (1973) Tectonic setting of basic volcanic rocks determined using trace element analyses. Earth Planet Sci Lett 19:290–300
Pearce JA, Peate DW (1995) Tectonic implications of the composition of volcanic arc magmas. Annu Rev Earth Planet Sci 23:251–285
Pearce JA, Baker PE, Harvey PK, Luff IW (1995) Geochemical evidence for subduction influxes, mantle melting and fractional crystallization beneath the South Sandwich island arc. J Petrol 36:1073–1109
Pearce JA, Kempton PD, Nowell GM, Noble RS (1999) Hf-Nd element and isotope perspective on the nature and provenance of mantle and subduction components in Western Pacific Arc-Basin system. J Petrol 40:1579–1611
Percival JA, Stern RA, Skulski T, Card KD, Mortensen JK, Begin NJ (1994) Minto block, Superior province: Missing link in deciphering assembly of the Craton at 2.7 Ga. Geology 22:839–842
Polat A, Kerrich R (1999) Formation of an Archean tectonic mélange in the Schreiber-Hemlo greenstone belt, Superior province, Canada: implications for Archean subduction-accretion process. Tectonics 18:733–755
Polat A, Kerrich R (2000) Archean greenstone belt magmatism and the continental growth-mantle evolution connection: constraints from Th-U-Nb-LREE systematics of the 2.7 Ga Wawa

subprovince, Superior Province, Canada. Earth Planet Sci Lett 175:41–54
Polat A, Kerrich R, Wyman DA (1998) The late Archean Schreiber-Hemlo and White River-Dayohessarah greenstone belts, Superior Province: collages of Oceanic plateaus, oceanic arcs, and subduction-accretion complexes. Tectonophysics 294:295–326
Polat A, Kerrich R, Wyman DA (1999) Geochemical diversity in oceanic komatiites and basalts from the late Archean Wawa greenstone belts, Superior Province, Canada: trace element and Nd isotopic evidence for a heterogeneous mantle. Precambrian Res 94:139–173
Puchtel IS, Hofmann AW, Mezger K, Jochum PK, Shchipansky AA, Samsonov AV (1998) Oceanic plateau model for continental crustal growth in the Archean: a case study from the Kostomuksha greenstone belt, NW Baltic Shield. Earth Planet Sci Lett 155:57–74
Rudnick RL (1995) Making continental crust. Nature 378:571–578
Sajona FG, Maury RC, Bellon H, Cotten J, Defant MJ, Pubellier M (1993) Initiation of subduction and generation of slab melts in western Mindanao, Philippines. Geology 21:1007–1010
Sajona FG, Maury R, Bellon H, Cotten J, Defant M (1996) High field strength element enrichment of Pliocene-Pleistocene island arc basalts, Zamboanga Peninsula, Western Mindanao (Philippines). J Petrol 37:693–726
Stein M, Hofmann AW (1994) Mantle plumes and episodic crustal growth. Nature 372:63–68
Stern CR, Kilian R (1996) Role of the subducted slab, mantle wedge and continental crust in the generation of adakites from the Andean Austral Volcanic Zone. Contrib Mineral Petrol 123:263–281
Stott GM (1997) The Superior Province, Canada, In: de Wit M, Ashwal LD (eds) Greenstone belts. Oxford Monogr Geol Geophys 35, Oxford, pp 480–507
Sun S-S, McDonough WF (1989) Chemical and isotopic systematics of oceanic basalts: implications for mantle composition and processes. In: Saunders AD, Norry MJ (eds) Magmatism in the ocean basins. Geol Soc Lond Spec Publ 42:313–345
Sun S-S, Nesbitt RW (1978) Petrogenesis of Archean ultrabasic and basic volcanics: evidence from rare earth elements. Contrib Mineral Petrol 65:301–325
Sylvester PJ, Campbell IH, Bowyer DA (1997) Niobium/Uranium evidence for early formation of the continental crust. Science 275:521–523
Taylor RN, Nesbitt RW (1998) Isotopic characteristics of subduction fluids in an intra-oceanic setting, Izu-Bonin Arc, Japan. Earth Planet Sci Lett 164:79–98
Taylor SR, Hallberg JA (1977) Rare-earth elements in the Marda calc-alkaline suite: an Archean geochemical analogue of Andean-type volcanism. Geochim Cosmochim Acta 41:1125–1129
Taylor SR, McLennan SM (1985) The continental crust: composition and evolution. Blackwell, Oxford
Taylor SR, McLennan SM (1995) The geochemical evolution of the continental crust. Rev Geophys 33:241–265
Thurston PC (1990) The Superior Province-emphasizing greenstone belts. In: Gold and base metal mineralization in the Abitibi Subprovince, Canada, with emphasis on the Quebec segment. Geol Dept (Key Centre) and Univ Ext, Univ Western Australia, Rep 24, pp 1–52
Thurston PC, Fryer BJ (1983) The geochemistry of repetitive cyclical volcanism from basalt through rhyolite in the Uchi-Confederation greenstone belt, Canada. Contrib Mineral Petrol 83:204–226
Thurston PC, Ayres LD, Edwards GR, Gelinas L, Ludden JN, Verpaelst P (1985) Archean bimodal volcanism. In: Ayres LD, Thurston PC, Card KD, Weber W (eds) Evolution of Archean supracrustal sequences. Geol Assoc Can Spec Publ 28:7–21
Thurston PC, Osmani LA, Stone D (1991) Northwestern Superior Province: review and terrane analysis. In: Thurston PC, Williams HR, Sutclife HR, Stott GM (eds) Geology of Ontario. Ontario Geol Surv Spec Vol 4(1):81–144
Williams HR, Stott GM, Heather KB, Muir TL, Sage RP (1991) Wawa Subprovince. In: Thurston PC, Williams HR, Sutclife HR, Stott GM (eds) Geology of Ontario. Ontario Geol Surv Spec Vol 4(1):485–539
Wilson M (1989) Igneous petrogenesis. Unwin Hyman, London
Wyman DA (1999) A 2.7 Ga depleted tholeiite suite: evidence for plume-arc inter-action in the Abitibi greenstone belt, Canada. Precambrian Res 97:27–42
Xie Q, Kerrich R, Fan J (1993) HFSE/REE fractionations recorded in the three komatiite basalt sequence, Archean Abitibi belt: implications for multiple plume sources and depth. Geochim Cosmochim Acta 57:4111–4118
Yogodzinski GM, Volynets ON, Koloskov AV, Seliverstov NI, Matvenkov VV (1994) Magnesian andesites and subduction component in a strongly calc-alkaline series at Piip volcano, far western Aleutians. J Petrol 35:163–204
Yogodzinski GM, Kay RW, Volynets ON, Koloskov AV, Kay SM (1995) Magnesian andesite in the western Aleutian Komandorsky region: Implications for slab melting and processes in the mantle wedge. Geol Soc Am Bull 107:505–519
Zaleski E, Peterson VL (1995) Depositional setting and deformation of massive sulphide deposits, iron formation, and associated alteration in the Manitouwadge greenstone belt, Superior Province, Ontario. Econ Geol 90:2244–2261
Zaleski E, Peterson VL, Lockwood H, van Breemen O (1995) Geology, structure and age relationships of the Manitouwadge greenstone belt, Northwestern Ontario. In: 41st Ann Meet Inst Lake Superior Geology, Marathon, Field Guideb 41(2b)
Zaleski E, van Breemen O, Peterson VL (1999) Geological evolution of the Manitouwadge greenstone belt and Wawa-Quetico subprovince boundary, Superior Province, Ontario, constrained by U-Pb zircon dates of supracrustal and plutonic rocks. Can J Earth Sci 36:945–966